Image-Based Quantification of Cell Size Variability in *S.aureus*: The Effect of Growth Rate

Thesis submitted towards the partial fulfilment of

BS-MS dual degree programme

By

Priyatham Pediredla

20091052

Under the guidance of

Dr. Chaitanya Athale

Assistant Professor

Division of Biology, IISER Pune

Certificate

This is to certify that this dissertation entitled “Image-Based Quantification of Cell Size Variability in *S. aureus*: The Effect of Growth Rate” towards the partial fulfillment of the BS–MS degree at the Indian Institute of Science Education and Research, Pune represents original research carried out by Mr. Priyatham Pediredla at IISER, Pune under the supervision of Dr. Chaitanya Athale, Assistant Professor, Biology Department during the academic year 2014-2015.

Dr. Chaitanya Athale **Date: 25/03/2015**

Assistant Professor

Div. of Biology, IISER Pune

Declaration

I hereby declare that the matter embodied in the report titled “Image-Based Quantification of Cell Size Variability in *S. aureus*: The Effect of Growth Rate” are the results of the investigations carried out by me at the Department of Biology, IISER Pune under the supervision of Dr. Chaitanya Athale and the same has not been submitted elsewhere for any other degree.

Priyatham Pediredla **Date: 25/03/2015**

20091052

BS-MS student

IISER Pune

Abstract

Variability in cell sizes is seen in isogenic bacterial populations despite of maintenance of cell size homeostasis. Quantification of cell sizes in a bacterial population can help us elucidate mechanisms that might disturb the size distribution in the community. Cell sizes have been quantified earlier in *E.coli* and found to be dependent on growth rate. This dependence results from multi-fork replication in fast growing *E. coli*. Here we quantified cell size variation in a *S. aureus* population and its dependence on growth rate.

We have developed and optimized an algorithm to detect spherical and ellipsoid cells in label-free DIC images in ImageJ. We assess the population density dependence of cell size variations in a batch culture and find no difference in the noise across different growth phases. Perturbing the cell cycle either with Cephalexin (cell division inhibitor) or with Hydroxyurea (DNA replication inhibitor) results in an increase in mean cell area of treated cells as compared to non treated cells. However no significant change in the phenotypic noise is observed.

This study sets the stage for a quantitative understanding of cell shape variability due to non-genetic factors, across strains in a gram positive coccal bacterium, thus complementing previous work on gram negative *E. coli*. It suggests that the observation of growth rate dependence on cell size variability could be a conserved mechanism.

Table of Contents

List of figures

Corrigendum

This is with regards to Error estimation figure in my dissertation, the error percentage provided in the thesis in page 13 was wrongly calculated and hence need replacement for the error percentage number as well as error estimation figures (Figure 9, Page 14).

The corrected figures and numbers are:

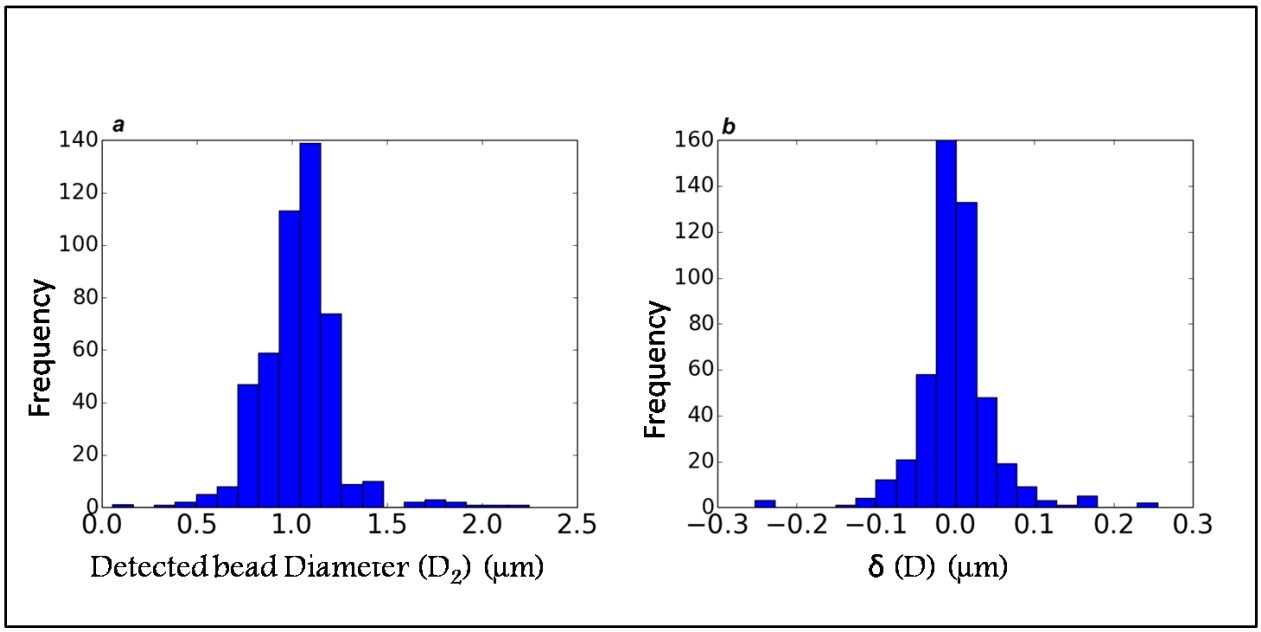

Figure 1: Frequency distributions of diameter of beads detected a: Distribution of detected bead diameters. b: distribution of difference between detected diameters of bead and actual diameter of beads

Text written in page 31 line 4- “The validation of our algorithm using beads showed, 7.4% error in the size measurement (Eq. 8), which leads to an offset of 0.074 µm from the actual diameter of the object” should be replaced with The validation of our algorithm using beads showed, 14.7% error in the size measurement (Eq. 8), which leads to an offset of 0.14 µm from the actual diameter of the object.

Acknowledgements:

I thank my mentor Dr. Chaitanya Athale for his constant support, invaluable guidance and bearing with me during my two years of research in his lab. I thank my TAC member Dr. Kota Miura for giving his valuable suggestions throughout my project. I take this opportunity to thank all my lab members for their constant encouragement and for creating a friendly ambience throughout my research project. Special thanks to my senior lab member Manasi Gangan (Ph.D. student) for guiding me throughout my project.

I thank all my friends for many sweet memories during my stay at IISER Pune. Special thanks to my parents for backing me during all my hard phases of life and for their unconditional love for me.

Finally I thank IISER Pune for providing modern research facilities at undergraduate level.

Introduction

Bacterial cell size and shape is governed by complex gene circuits, the expression of which is fine tuned by the growth rate determined by their niche. Asexual cell division in microorganisms generates a population of clonal cells, which are expected to exhibit an identical phenotype. In bacterial cells, cell size homeostasis is critically maintained. According to the growth law, cells in exponentially growing phase are supposed to be bigger than cells in resting phase, or in other words cell volume increases as a function of growth rate imposed by nutrient (Schaechter et al., 1958). This was supported by the results of studies done on *Salmonella typhimurium,* where it was shown that cell mass is an exponential function of growth rate at a particular temperature (Schaechter et al., 1958). Based on the growth law, several models have been postulated to explain the cell size homeostasis. According to the 'sizer' model elongation depends on the birth size of a cell and the cell cycle is triggered after bacteria reach their critical size (Chien et al., 2012). The alternative 'timer' model states that cell grows for some time before division, and is independent of birth size (Osella et al., 2014). However the analysis of gram negative *Escherichia coli* and gram positive *Bacillus subtilis* under variable growth conditions supported the 'adder' model which states that cells adds certain volume after each generation which is independent of birth size (Amir, 2014). This was investigated at population level as well as at the single cell level in both the bacteria (Taheri-Araghi et al., 2014)

Despite of cell size homeostasis maintenance, variation in length is often seen in an isogenic population of bacteria. Previous experiments attributed phenotypic variations either to the fluctuations in gene expressions or due to the changes in external environmental conditions. At the gene-expression level, much interest has focused on gene expression variability. An *E. coli* strain with equidistant genomic insertions of CFP and YFP encoding genes from oriC and expression under pLac control showed enhanced difference in fluorescent protein intensities in the absence of lactose (Elowitz et al., 2002). The difference in the intensities reduced post Isopropyl

thiogalactopyranoside: IPTG (which inactivates *lac* repressor) (Figure 1a). Micro colonies of *S. typhimurium* strain in which GFP encoding gene was cloned downstream to the native promoter of FliC (responsible for flagellar expression) showed varied GFP expression which can be interpreted as fluctuations in flagellar expression (Figure 1b) (Freed et al., 2008). Apart from the fluctuations in gene expression, changes in environmental conditions are also shown to cause phenotypic variability in clonal populations. For instance cell volume has been shown to increase in *E.coli* with decreasing temperature from 37 ºC to 22 ºC (Shehata and Marr, 1975) and cell lengths were found to be comparatively shorter in *E.coli* grown at 22ºC compared to the same bacteria grown at 37ºC (Trueba et al., 1982).

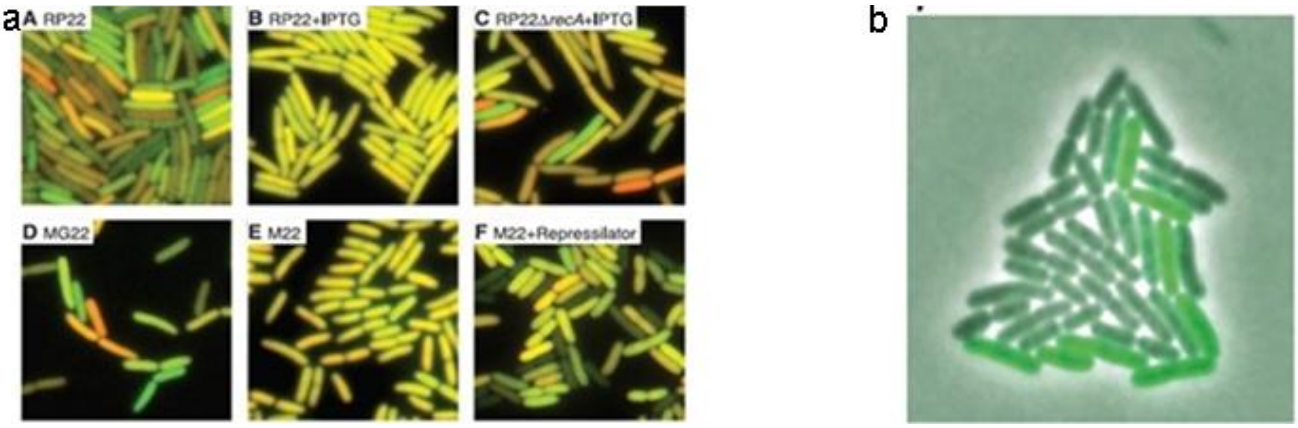

Figure 2: Gene expression noise studied in bacteria. a: Noise in *E.coli* due to stochastic gene expression. CFP protein: green, YFP protein: red, Merge: yellow (taken from Elowitz et al., 2002). b: Noise due to fliC promoter leading to various levels of expression of GFP (green) in *S.typhimurium* grown from a single cell (taken fromFreed et al., 2008).

Earlier in the Athale-lab variation in cell lengths of functional Rec A mutants of *E. coli* (DH5α and HB101) was observed as compared to the wild type bacteria, and found to be growth phase dependent (Gangan et al. submitted). Cell sizes were extracted from DIC images of *E. coli* using MATLAB code developed (Athale and Chaudhari, 2011) and the cell length distribution was found in rare instances to exceed 25 µm in recA mutants and 10µm in wild type strain. However in most strains, the modal values of the distributions were comparable at ~2 µm (Figure 2a). Number of nucleoids observed in

the laboratory strain DH5α showed a linear correlation with cell lengths with a slope of around 2.2 µm which is almost equal to the cell size at birth, indicating that nucleoid segregation and cell elongation are not affected, but cell septation inhibited in long cells (Athale and Chaudhari, 2011). In other studies, *E. coli* cells were treated with Hydroxyurea known for inhibition of ribonucleotide reductase (RNR) enzyme and hence the inhibition of de novo synthesis of dNTP's. The depletion of dNTPs halts DNA replication, which in turn, delays and inhibits cell division (Margolin, 2000) culminating into cell elongation (Figure 2b). Inhibition of cell division in bacteria is done by affecting the polymerization of FtsZ protein (assembles to form a ring at future site of cell division). The molecular mechanisms identified so far that regulate cell division include (1) MinCDE system in *E. coli* and MInCD- DivIV in *B.subtilis* that inhibit division at cell poles (Barakand Wilkinson, 2007) (2) SlmA in *E.coli* (Bernhardt and De Boer, 2005) and Noc in *B subtilis* (Wu and Errington, 2004) popularly known as nucleoid occlusion system, causing inhibition of Z- ring formation over unreplicated or unsegregated chromosomes. Nucleoid occlusion was shown to prevent cell division in *B. subtilis* during replication fork stalling (Bernard et al., 2010). Also (3) a branch of RecA mediated SOS response pathway in which synthesis of SulA protein after replication fork stalling at DSBs sequester FtsZ monomers and prevent the cell division (Bi and Lutkenhaus, 1993). Last two mechanisms are important in pairing between DNA replication and cell division.

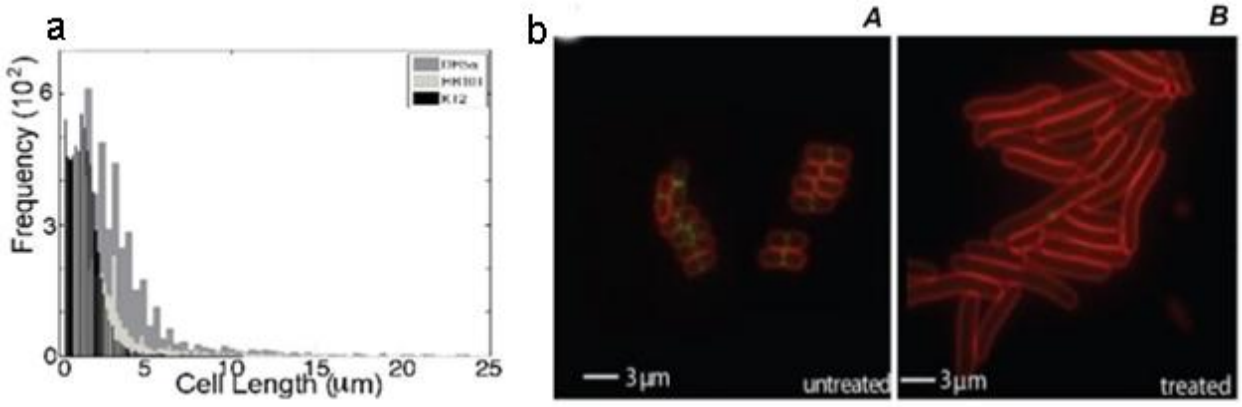

Figure 3: Variation in cell length of E.coli. a: Rec A mutant strain Dh5α shows variation in cell lengths as compared to wild type strains (taken from Athale and Chaudhari, 2011). b: A-

Untreated *E. coli* showing normal cell sizes, B-Hydroxyurea treated cells showing larger cell sizes due to inhibition of division (taken from Margolin, 2000).

The project is motivated by a need to characterize the population phenotypic variability in *S.aureus* as a function of growth rate, to see if the replication fork dependent mechanism is also seen in this bacterium. *S.aureus* is a gram positive, spherical bacterium. It is a normal flora of human skin and is a well- known opportunistic pathogen and has medical importance. When grown in artificial media it divides to form a grape bunch like clusters (Tzagoloff and Novick, 1977) (Figure3), which is mainly because of its cell division in three dimensional planes perpendicular to each other (Figure 4). In rod shaped bacteria like *E.coli* and *B. subtilis*, MreB related proteins are shown to be responsible for elongated morphology (Jones et al., 2001). The absence of MreB-like proteins in *S.aureus* could be the cause for its spherical shape. Generality among bacterial species can be established if growth phase dependence of phenotypic variability in *S.aurues* is observed similar to that of in *E.coli* (Athale and Chaudhari, 2011). Depletion of FtsZ protein in *S.aureus* has shown to be forming filamentous cells with no septa (Pinho and Errington, 2003).Division plane is not well defined in *S.aureus*, like other bacteria though it was recently speculated that the cell uses epigenetic information in the cell wall to label division planes (Turner et al., 2010). *S.aureus* does not have any Min system, recently it was shown that Z ring is formed over nucleoids upon deletion of Noc in *S.aureus* (Figure 5) and it was postulated that chromosome segregation plays a crucial role in Z ring formation and selection of dividing plane (Veiga et al., 2011).

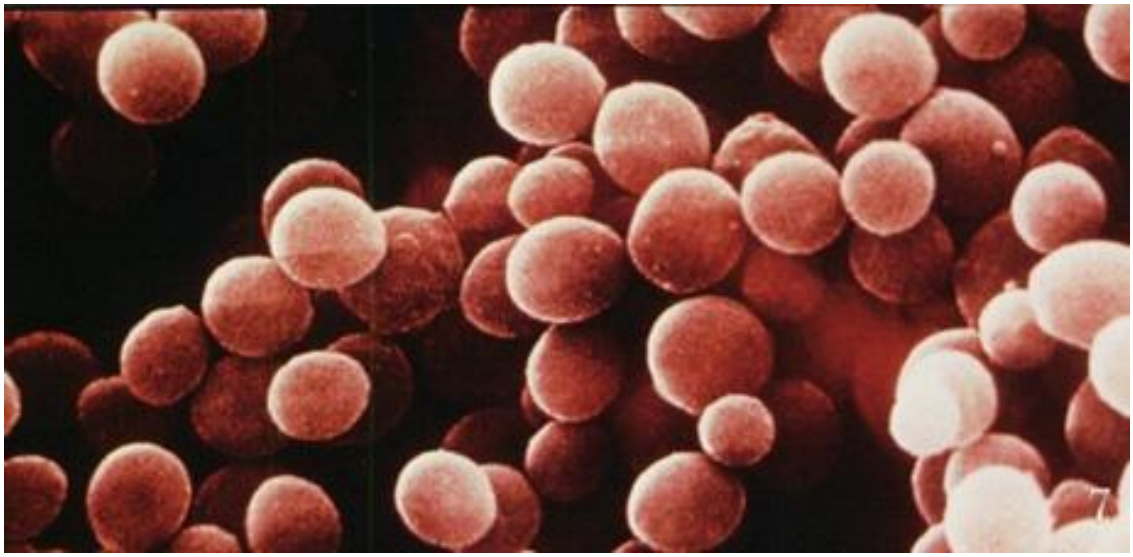

Figure 4: *Staphylococcus aureus.* Electron micrograph of *S.aureus*, show them dividing in three planes and forming bunch like structure (taken from Todar (2008-12))

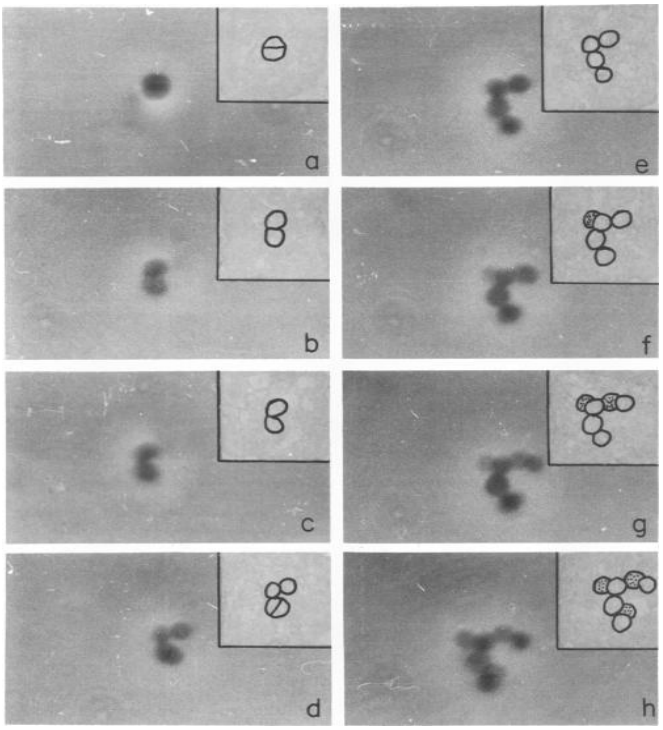

Figure 5: Division of *S.aureus* in three planes. Phase contrast images of bacteria dividing in three dimensions with diagrammatic representation of formation of clump (taken from Tzagoloff and Novick, 1977).

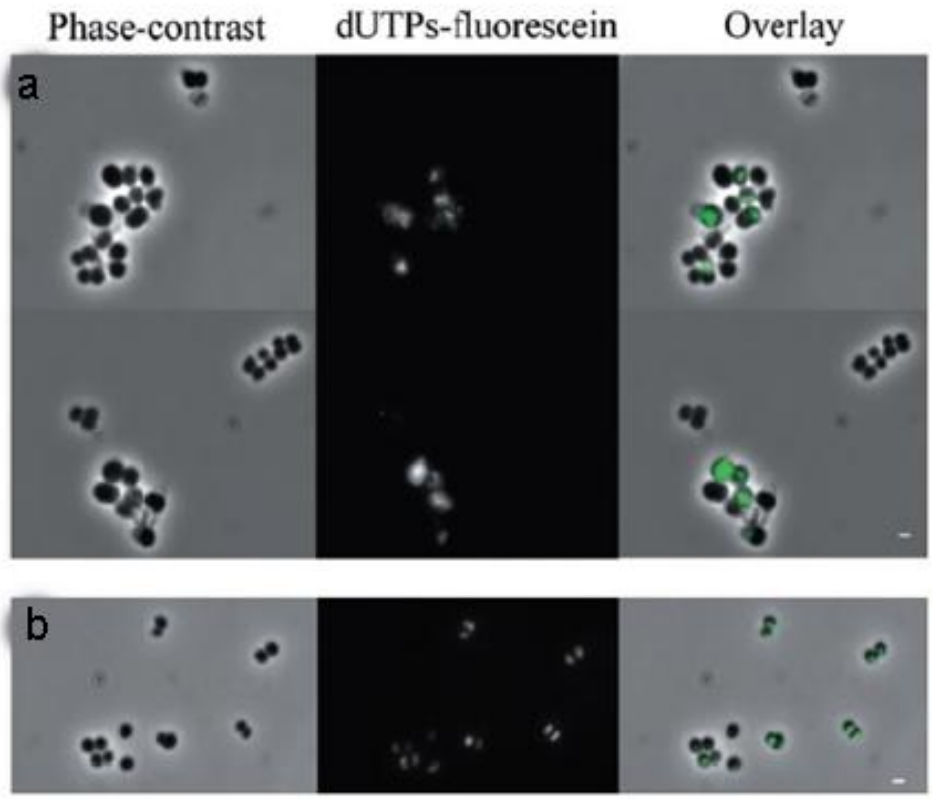

Figure 6: Noc deletion in *S.aureus* leading to DNA breakage. a: Noc deleted cells. b: Wild type cells. Left Panel: Phase contrast images, Middle Panel: Fluorescent image of dUTP incorporated in DNA breakage, Right Panel: Overlay image of phase contrast and fluorescent image (taken from Veiga et al., 2011).

Here, we have developed a tool to detect *S.aureus* cell size distributions in DIC. When *S. aureus* cultures were grown in liquid batch culture under optimal conditions and analyzed for cell size variation in growth phase dependent manner, we find no significant difference in the phenotypic noise with increasing population density. Based on perturbation experiments using Hydroxyurea and Cephalexin, we proceed to test the hypothesis that the stochasticity in DNA replication leads to phenotypic variability in an isogenic population of *S. aureus* as it effects the cell division.

Materials and Methods

Bacterial Strain

The strains used in the study were *Staphylococcus aureus* (5022, NCIM, NCL, Pune).

Bacterial Growth

1% inoculum from overnight grown culture of *S. aureus* was inoculated into fresh sterile Nutrient Broth (NB) (1.3 g in 100 ml of de-ionized water) (HiMedia, Mumbai) either diluted with 1X phosphate buffered saline (PBS, ph = 7.4) or without dilution and incubated at 37ºC with continuous shaking at 180 rpm (Thermo scientific orbital shaker, Germany). The cellular growth was monitored using optical density (O.D) at 600 nm (Eppendorf, Biophotometer, and 8.5 mm Light center height, Germany) at regular intervals. Bacterial cell samples for respective time points were collected in triplicates.

Cephalexin Treatment

1% primary culture was inoculated in fresh NB and grown till O.D reached 0.4. Cephalexin (SRL, Mumbai) was then added to the culture to a final concentrations of 1 µg/ ml or 3 µg/ml suspended in de-ionized water and re- incubated at 37°C at 180 rpm (Innova 4230, New Brunswick Scientific, Germany) for 3 hours, aliquots were taken after every 30 minutes after the Cephalexin addition.

Hydroxyurea (HU) Treatment and Recovery

1 % primary culture was inoculated in fresh NB and grown till O.D reached 0.4. Hydroxyurea (Thermo fisher scientific, Germany) was added to the culture and was incubated at 37°C for 5 hours; aliquots were taken for every hour and stored aside. Two concentration of Hydroxyurea were used: 10 mM and 25 mM suspended in de-ionized water. After 3 hours of HU treatment, 1ml of aliquot was taken, pellet down, washed

with PBS, re-suspended in 1ml of fresh NB and was incubated for two hours at 37°C with continuous shaking at 180 rpm, aliquots were taken after every one hour.

Sample Preparation

Aliquots were pelleted down (Eppendorf, centrifuge 5424 R, Germany) for 30s at 13000 rpm and washed twice with PBS, cells were fixed by incubating them with 4% Para formaldehyde (PFA) suspended in de-ionized water (Sigma-Aldrich, USA) and kept at room temperature for 30 minutes. After final wash with PBS, cells were re-suspended in 100 µL of PBS. For staining the nucleoids 1 µg/ml DAPI (SRL, Mumbai) was added to the aliquots after fixing with PFA and incubated for 5 minutes, 4 µl of the above sample was smeared on a microscopy slide of size 75x22 mm (MicroAid, India) dried and mounted with 3µl of the mountant. The smear was then sealed by placing cover slip (Micro Aid, 22x22 mm, India) which was cleaned before placing with 70% Ethanol, over it.

Microscopy

Fixed samples were imaged with an epifluorescence, Zeiss AxioImager Z.3 (Carl Ziess, Germany) upright microscope with a white light source (100W) using a 100x lens, NA =1.3 (scaling factor, 1 Pixel = 0.05 µm). Images were acquired using the Zeiss Image acquisition program (Axiovision ver.4.8) in the DIC and fluorescence modes. The filter cube sets for DAPI excitation (358 nm) and emission (461 nm) were used for fluorescence measurements based on a mercury short arc lamp light source (X-Cite Series 120, Lumen Dynamics Inc., and Canada.)

Growth Rate Estimation

Growth curves of *S. aureus* in liquid medium were measured using O.D. 600nm and plotted in MS Excel 2007 (Microsoft Corp., USA). The doubling time was calculated using the following formula:

$$B = A \times 2^{n} \qquad \text{Eq. 1}$$

$$\log (B) = \log (A) + n \log 2$$

$$n = \frac{\log (B) - \log (A)}{\log (2)}$$

$$n = 3.3 \log (B/A) \qquad \text{Eq. 2}$$

$$\mathbf{G = t/n} \qquad \text{Eq. 3}$$

Where,

t = time interval in hours or minutes

A = number of bacteria at the beginning of a time interval

B = number of bacteria at the end of the time interval

n = number of generations.

G = generation time.

The O.D.600nm measurements were converted into cell density using a conversion factor of 1OD= $1x10^8$ CFU/ml (Watson et al., 1998) seen previously to obtain a cell density value as a function of time. The values of A and B were chosen from the log (cells/ml) plots (Figure 10) as a function of time based on the linear region of the growth curve indicative of log-phase.

Image Analysis

An algorithm (Appendix 1) was devised in ImageJ 1.46r with Java 1.6.0_20 (32 bit) (Rasband, 2012) platform to process raw DIC images of cells obtained from the microscopy, strategy was to get rid of the shadow of the cells in DIC, subtract background and segment (Roerdink and Meijster, 2000) the images. Fluorescent images were processed to get rid of the noise in the background. To test the robustness of the algorithm, it was applied to estimate cell areas and compared to the manual estimation for the same cells. The manual estimation was averaged mean over 3 persons. Additionally DIC images of 1 μm diameter polystyrene beads (Bangs

laboratories, USA) mounted in cell-mountant were analyzed using the algorithm and results were compared.

Cell size parameters were obtained from the processed images in Enthought-Canopy (Version 1.3.0 for 32 bit) using Python (2.76 Version). Size parameters were pooled together and their frequency distributions were plotted in Matlab (R 2010b). Lognormal curves were fitted to these frequency distribution plots by a previously developed code in our lab using MATLAB (Appendix 2).

The lognormal distribution of a dataset x is given by

$$\boldsymbol{f(x) = \frac{1}{x\sigma\sqrt{2\pi}} e^{\frac{-\ln(x-\mu)^2}{2\sigma^2}}} \quad \text{Eq. 4}$$

Where, μ and σ are mean and standard deviation of $\ln(x)$.

Goodness of the fit was tested by using Kolmogorov-Smirnov test (Wilcox, 1998). A statement of no difference between observed values and expected values is considered as null hypothesis: H_0 and if null hypothesis is false then alternative hypothesis: H_A is assumed to be true.

Equation used for KS test is:

$$\boldsymbol{D(\alpha, n) = \sqrt{(-\ln(\alpha/2))/2n}} \quad \text{Eq. 5}$$

Where $\boldsymbol{\alpha}$- significance value (0.01) and n- total no of objects.

$$\mathrm{d} = \max\ (\mathrm{F1} - \mathrm{F2}) \quad \text{Eq.6}$$

Where, F1= cumulative observed frequencies and F2= cumulative expected frequencies.

d > D indicates rejection of null hypothesis.

Coefficient of variation (CV) was calculated from the mean and the standard deviation of the dataset and was plotted.

Following formula was used to calculate the coefficient of variation:

$$\boldsymbol{Cv = \frac{\sigma}{\mu}} \quad \text{Eq. 7}$$

Where,

Cv - Coefficient of variation

σ - Standard deviation

μ - Mean.

For calculating percentage error, the following formula was used:

$$\%error = \frac{\#experimental - \#theoretical}{\#theoretical} .100 \qquad \text{Eq. } 8$$

Where,

#experimental – Value obtained after performing experiment

#theoretical – Standard value.

Results

Algorithm Devised

DIC images obtained from the microscopy were processed with an algorithm devised in ImageJ. Strategy was to reduce the background noise in the images for which median filtering was used, and to overcome the shadow formed in DIC images maximum filtering was used, OTSU threshold was applied on the filtered images and they were segmented using watershed, outline of the processed images were overlaid on raw DIC images and outline looked to be fitted on the raw images (Figure 6). Processed images were analyzed to estimate cell area.

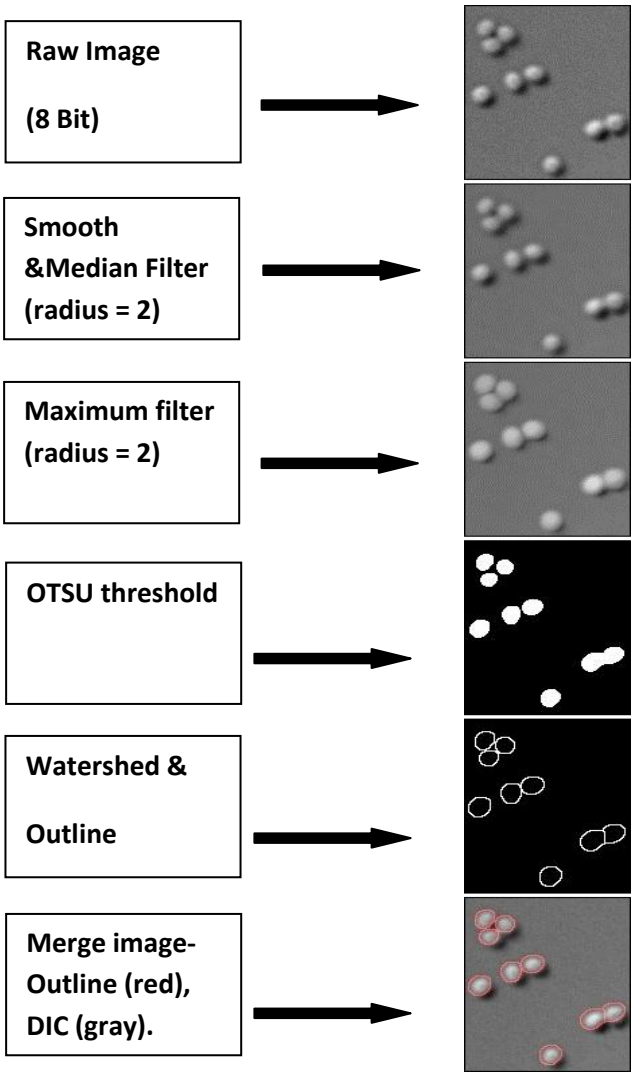

Figure 7: Flow chart of algorithm devised in ImageJ. Individual steps on the left side in the text boxes from top to bottom with corresponding images after applying each step on the right side.

The validity of the algorithm was tested by comparing cell areas obtained from algorithm: A_a with cell area measured manually: A_m (averaged over measurements of three persons), A_m was considered to be standard measurement and was calculated using free hand detection tool in ImageJ. The slope of a straight line fitted to the data points was 1.01 and R squared (R^2) value was found out to be 0.994 indicating that regression line is almost perfectly fitting to the data (Figure 7).

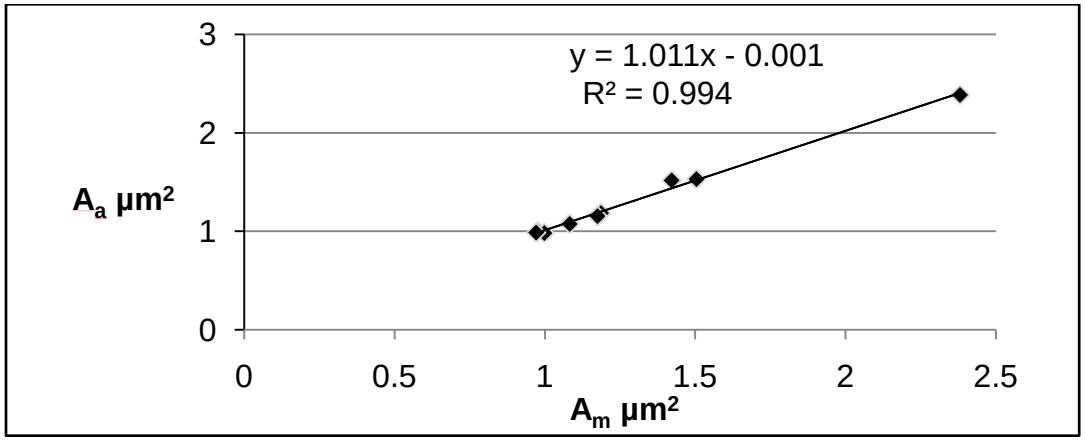

Figure 8: Algorithm validation with manual detection. Area obtained with algorithm- A_a (μm^2) on 'Y'-axis, manually detected area- Am (μm^2) on 'X' axis (averaged over n=3 persons).

To estimate the error in the detection made by algorithm, it was run on DIC images of beads of diameter 1 µm (Figure 8). An error percentage (Eq. 8) of 7.4 is found. Frequency distributions of diameters of beads obtained from algorithm were plotted, the modal value of the distribution is found to be in between 1 µm – 1.2 µm, while the diameter was found to varying between 0.7 µm – 1.4 µm (Figure 9a), frequency distribution of d (D) (difference between diameter obtained from the algorithm and actual diameter of bead) was plotted and modal value was found to be in the range of 0 µm – 0.2 µm (Figure 9b).

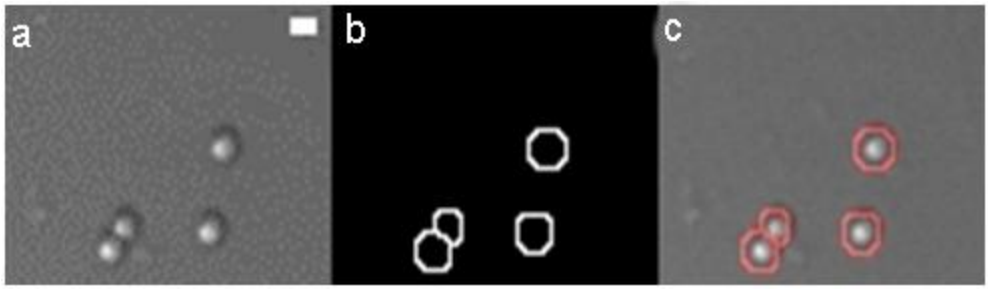

Figure 9: Testing algorithm on beads. a: DIC images of beads, b: outline of beads detected by the algorithm and c: merge of outline (red) with DIC (gray) images of beads. Scale bar = 1 µm

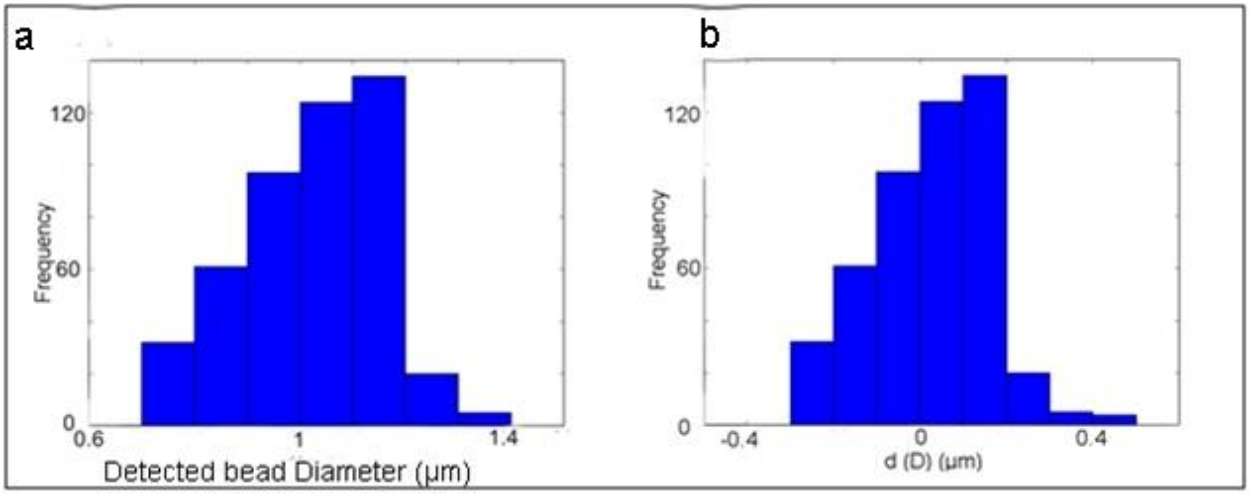

Figure 10: Frequency distributions of diameter of beads detected a: Distribution of detected bead diameters. b: distribution of difference between detected diameters of bead and actual diameter of beads.

Modulation of Bacterial Growth Rate

To study growth rate dependence of phenotypic variability of *S.aureus*, population growth rate was modulated by changing the nutrient availability. Growth of *S. aureus* in NB and diluted NB with time has been depicted in Figure 10. Average doubling time of the population was calculated for growth between data points ‘A’ and ‘B’ (Figure 10) and doubling times were depicted in bar graphs along with change in media concentration in Figure 11. Samples corresponding to different growth phases (early log, mid log and

stationary) depicted by encircled points in Figure 10 were chosen for imaging (Figure 12).

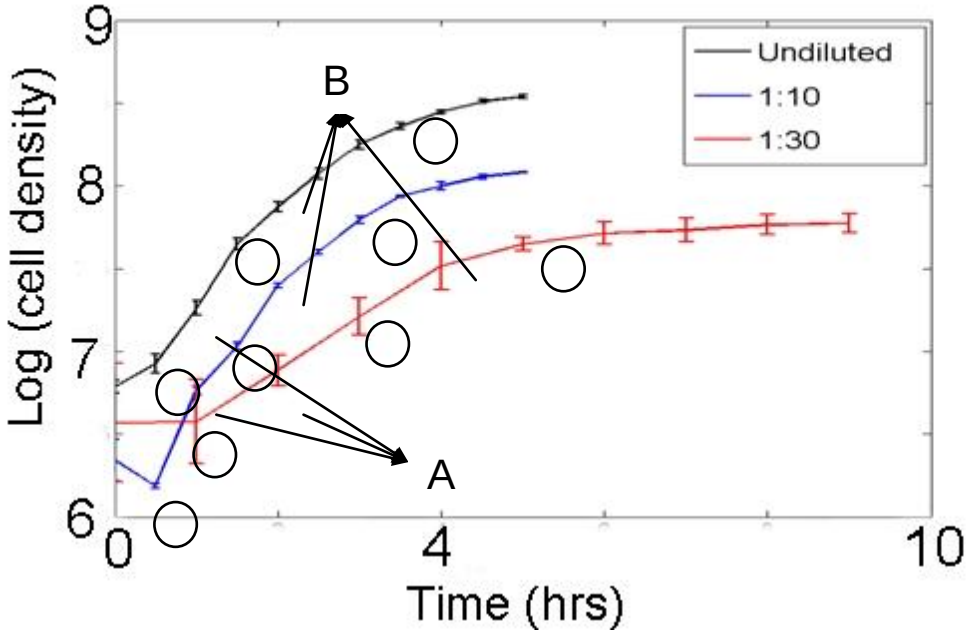

Figure 11: Growth curve of S.aureus. Time in hours on X-axis and cell density on Y-axis in logarithmic scale (n=3). Samples corresponding to circled points were taken for imaging. ‘A’ and ‘B’ are points chosen for calculating doubling times.

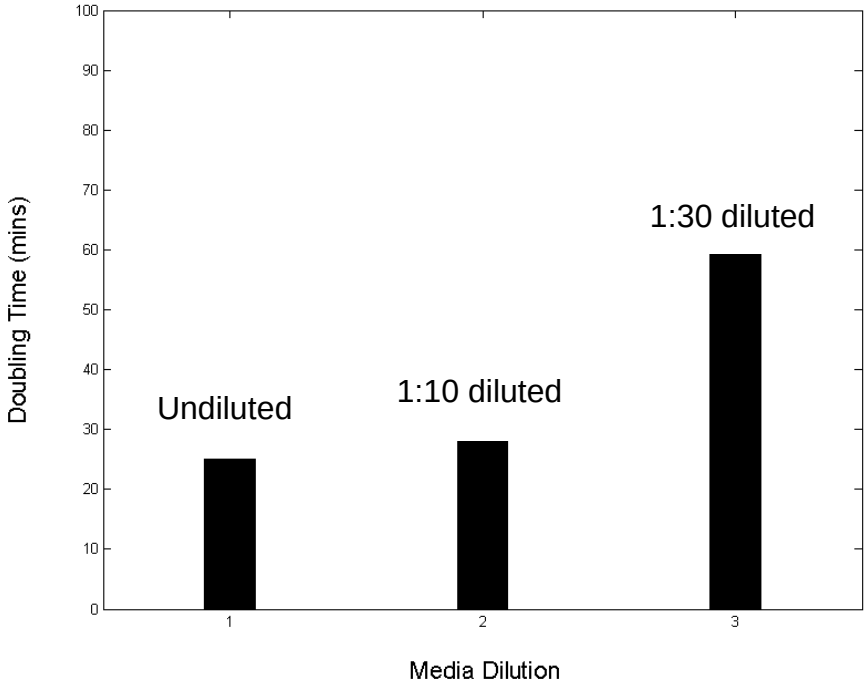

Figure 12: Doubling times of bacteria grown under different concentrations of media. Media dilution on X-axis and doubling time on Y-axis. Doubling time was calculated between points A and B as indicated in the Figure 10 (Eq.2 and Eq.3).

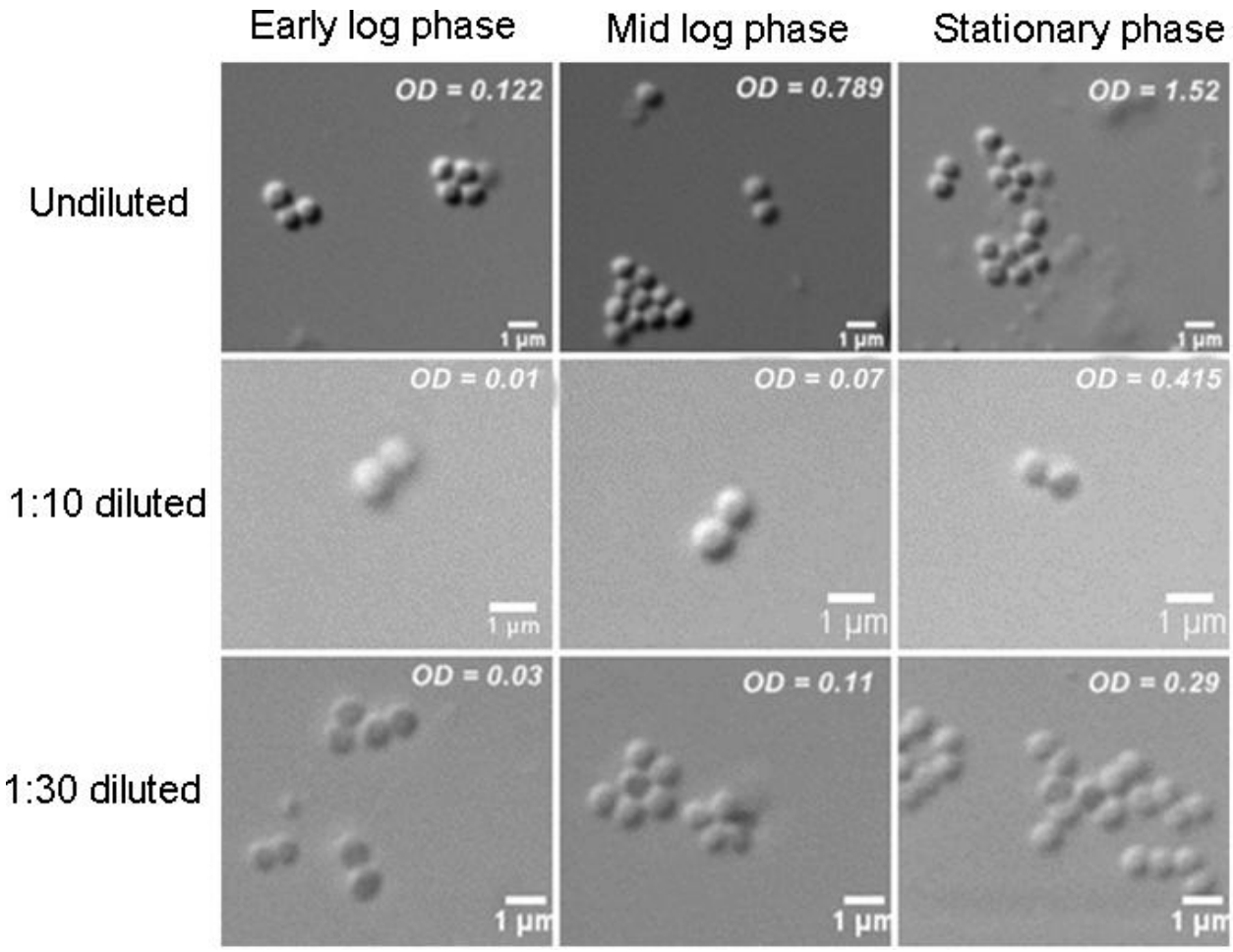

Figure 13: DIC images of *S.aureus* cells. Snapshots of DIC images of cells with changing growth phase (left to right) and with changing media dilution (top to bottom). Scale bar = 1 µm.

Frequency distributions of the cell area assessed using algorithm were plotted for corresponding population densities (Figure 13). No significant chage in the mean cell area was observed along the growth phase in all three growth conditions, variance is also found to be similar in all phases. Frequency distribution plots were fitted with

lognormal distribution and to test the goodness of the fit, KS test was performed, d value was found to be lesser than D indicating that null hypothesis (expected data is same as observed data) holds, however d>D was observed in frequency distribution plots of areas fitted with lognormal fits for samples taken from stationary phase which were grown in undiluted media indicating that the expected data doesnot match with observed data at significance value of 0.01.

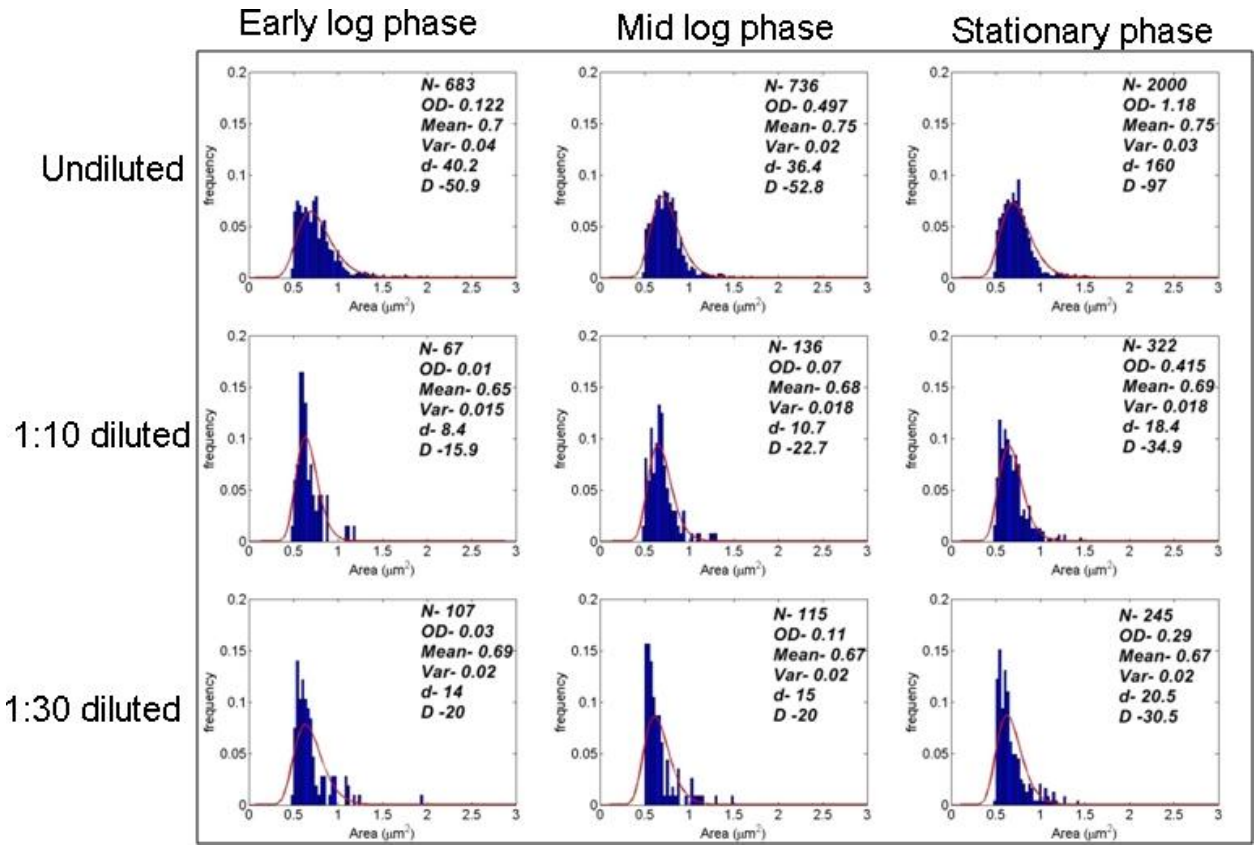

Figure 14: Frequency distribution of areas of cells. Frequency histograms (sum normalized) of Area (μm^2) on X axis fitted with lognormal distributions for cells taken from the different growth phases (left to right) and from the different media concentrations (top to bottom). N corresponds to the number of samples analyzed, Mean- logarithmic mean of the samples, Variance- logarithmic variance of the samples, d- KS test, and D-KS test.

.

To measure the noise in cell size, coefficient of variation (CV) was calculated for cell areas and was plotted as a function of time (Figure 14), in undiluted and 1:10 diluted samples CV showed higher initial values which correspond to the early log phase of the growth as indicated by the time, and then gradually decreased, however the change is very less, in 1:30 diluted samples CV value was found to be constant for all growth phases. CV of samples taken from particular growth phase from different growth conditions were plotted with doubling times (Figure 15), value of CV is found to be decreasing with increasing doubling time (from 25 mins to 35 mins) for samples taken from all three phases but the change in the values was not so significant.

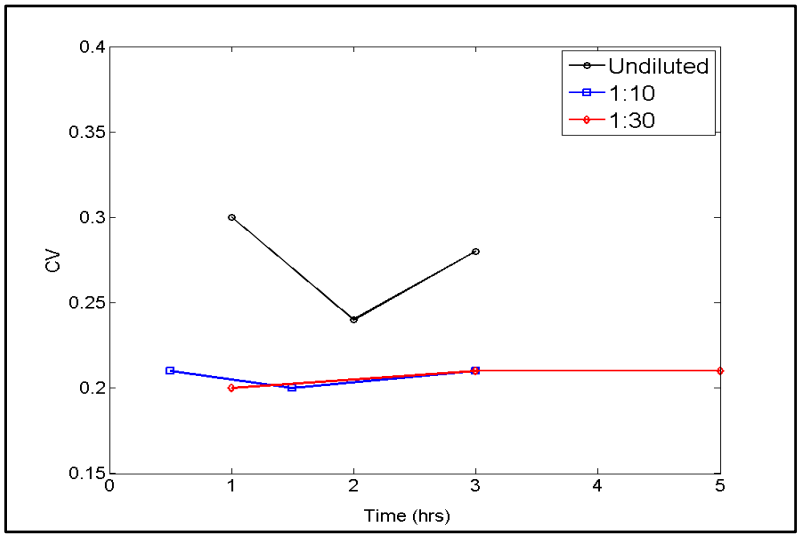

Figure 15: Change in coefficient of variation (CV) with growth phase. Coefficient of variation (CV) of area on Y-axis. Time (hours) on X-Axis.

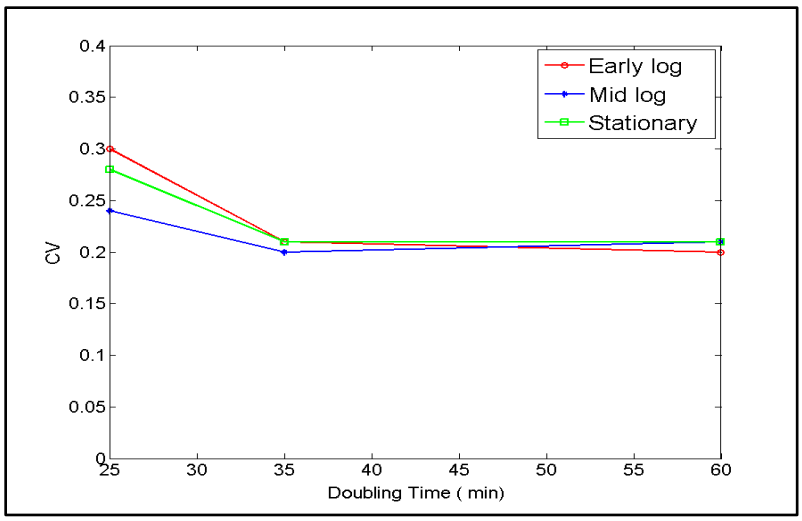

Figure 16: Change in coefficient of variation (CV) with doubling time. Coefficient of variation (CV) of area on Y-axis. Doubling time (mins) on X-Axis.

Drug treatment

Cephalexin Treatment

To study the effect of delayed cell division on the cell area distribution, we treated the cells with Cephalexin which inhibits cell division by repressing the function of FtsI protein. Two different concentrations of Cephalexin were used in this study: 1µg/ml and 3 µg/ml. Cell size seems to be increasing from 0:00 hours to 4:00 hours in the DIC images (Figure 16a and Figure 17a). Nucleoid segregation was examined by imaging DAPI stained nucleoids in these cells (Figure 16b and Figure 17b). Nucleoids were observed to be segregated in the enlarged cells even after 240 minutes of 3µg Cephalexin treatment (Figure 17b). Cell area distributions were plotted and fitted with lognormal function. We observed that mean cell area was found to be increasing till 2hours of Cephalexin treatment. But surprisingly, it is found to be decreasing after 3hours (Figure 18a), d value was found to be less than D value in all the fits indicating that the data obtained follows lognormal distribution (Figure 18).

Though, the Coefficient of Variation of 1 µg/ml Cephalexin treated samples did not show any particular pattern as compared to that of untreated samples but showed monotonous decrease after 2hours which is correlated to decrease in mean cell areas

for same time points (Figure 19a). However, in the 3 µg/ml treated samples, a zigzag trend of coefficient of variation was observed (Figure 19b).

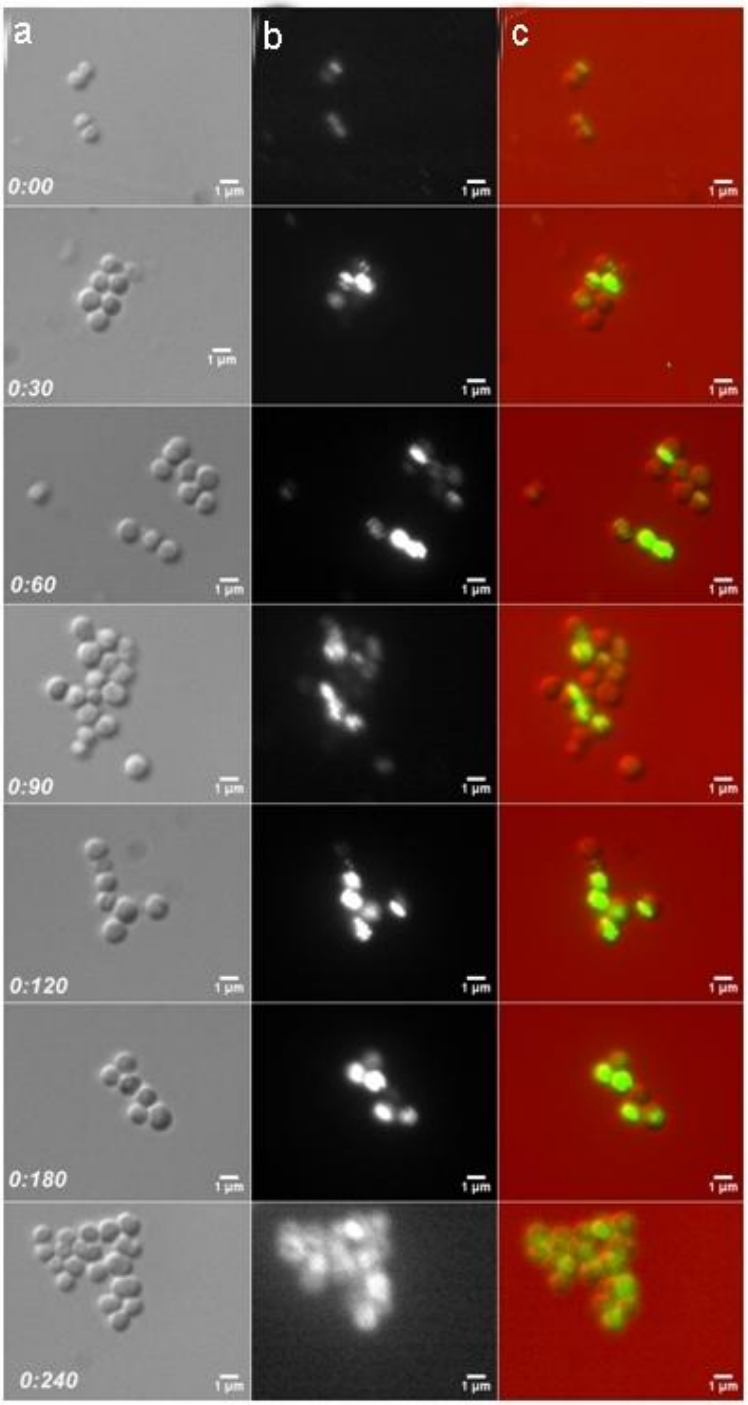

Figure 17: Effect of Cephalexin (1µg/ml) treatment on cells. a- Time series of DIC images of *S.aureus* cells treated with 1 µg/ml Cephalexin (starting from 0:00 mins: untreated to 0:240

mins). b- Florescent images of DAPI stained nucleoids. c- Overlay of florescent image in green with DIC images in red. Scale bar =1 µm.

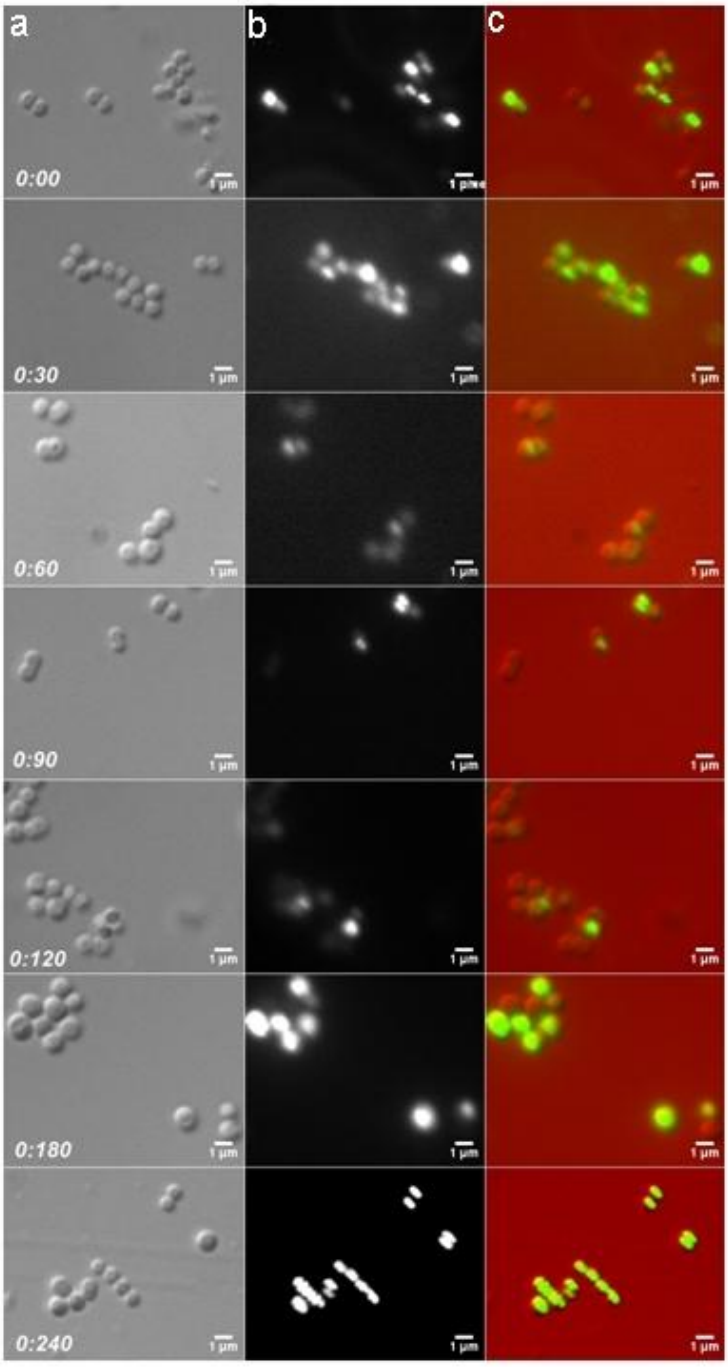

Figure 18: Effect of Cephalexin (3 µg/ml) treatment on cells. a- Time series of DIC images of *S.aureus* cells treated with 1 µg/ml Cephalexin (starting from 0:00 mins: untreated to 0:240

mins). b- Florescent images of DAPI stained nucleoids. c- Overlay of florescent image in green with DIC images in red. Scale bar =1 µm.

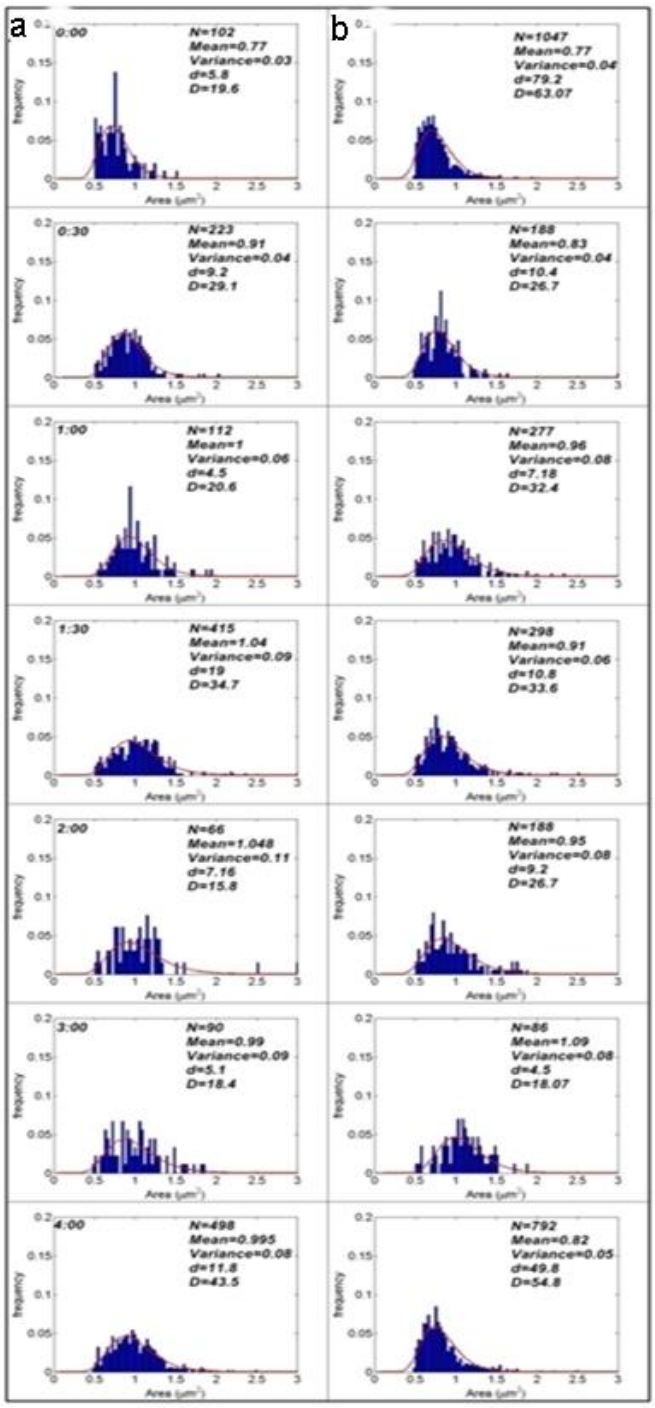

Figure 19: Frequency distribution plots of areas of cells treated with Cephalexin. Area histograms of treated with 1µg/ml (Panel a) and 3 µg/ml (Panel b) Cephalexin. Areas on X axis in μm^2, frequency (sum normalized) on Y axis. N-number of samples analyzed, Mean- Mean of

the samples, Variance- Variance of the samples, D- test statistic (Eq. 5), d- deviation from the fit (Eq. 6).

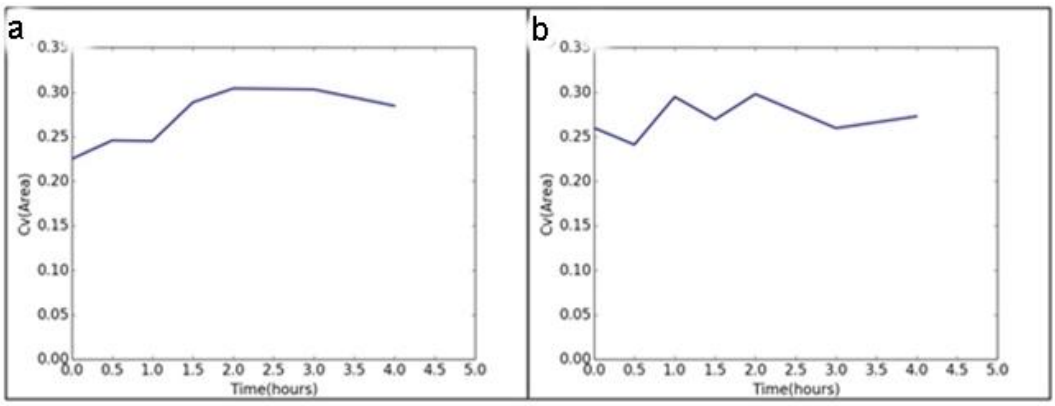

Figure 20: Coefficient of variation (CV) plots of Cephalexin treated cells. Cephalexin treated samples, a-1 µg/ml and b-3 µg/ml. Time (hours) on X-axis and Coefficient of Variation (CV) of area on Y-axis.

Hydroxyurea Treatment

To observe the effect of halted DNA replication on cell size variation, we treated the cells with Hydroxyurea, a chemical known to inhibit RNR enzyme essential for conversion of NTPs into dNTPs in de Novo synthesis of dNTPs. We chose two different concentrations of Hydroxyurea: 10 mM and 25 mM. DIC images of the cells show undivided bacteria of abnormal sizes along the time course compared to the untreated cells, however after 5 hours of treatment, survivors seem to retrieve the normal size and their cell areas are comparable to that of untreated samples (Figure 20a and Figure 21a). Nucleoids were observed along the time course for both treatments and some of them were not segregated properly (4:00 hrs Figure 20b, 3 & 4hrs Figure 21b) while most of them were segregated properly (Figure 20b and Figure 21b).

In the frequency distribution plots no significant change in the mean area was observed however long fat tail was seen in the plots of treated samples compared to untreated ones (Figure 22), d value was found to be lesser than D value for all plots fitted with lognormal distribution indicating that the data follows lognormal distribution (Figure 22).

Coefficient of variation seems to be increasing for both treatments till 3:00 hours of treatment compared to untreated (0 hours) and decreasing at 3rd hour, increasing in 4th hour and then decreasing (Figure 23).

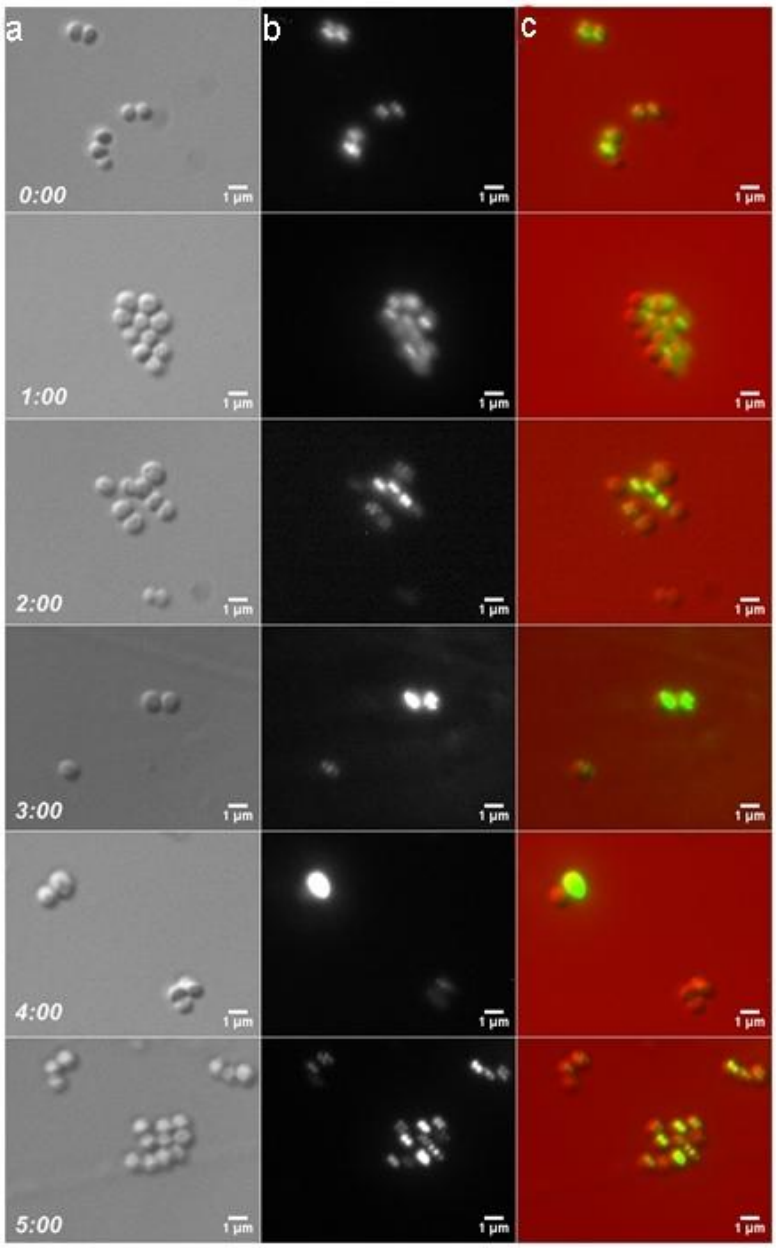

Figure 21: Effect of Hydroxyurea (10 mM) treatment on cells. a- Time series (0:00 – 5:00) of DIC images of *S.aureus* cells treated with Hydroxyurea (10 mM) with 0:00 hrs- untreated. b-

Florescent images of DAPI stained nucleoids. c- Overlay of florescent image in green with DIC images in red. Scale bar =1 µm.

.

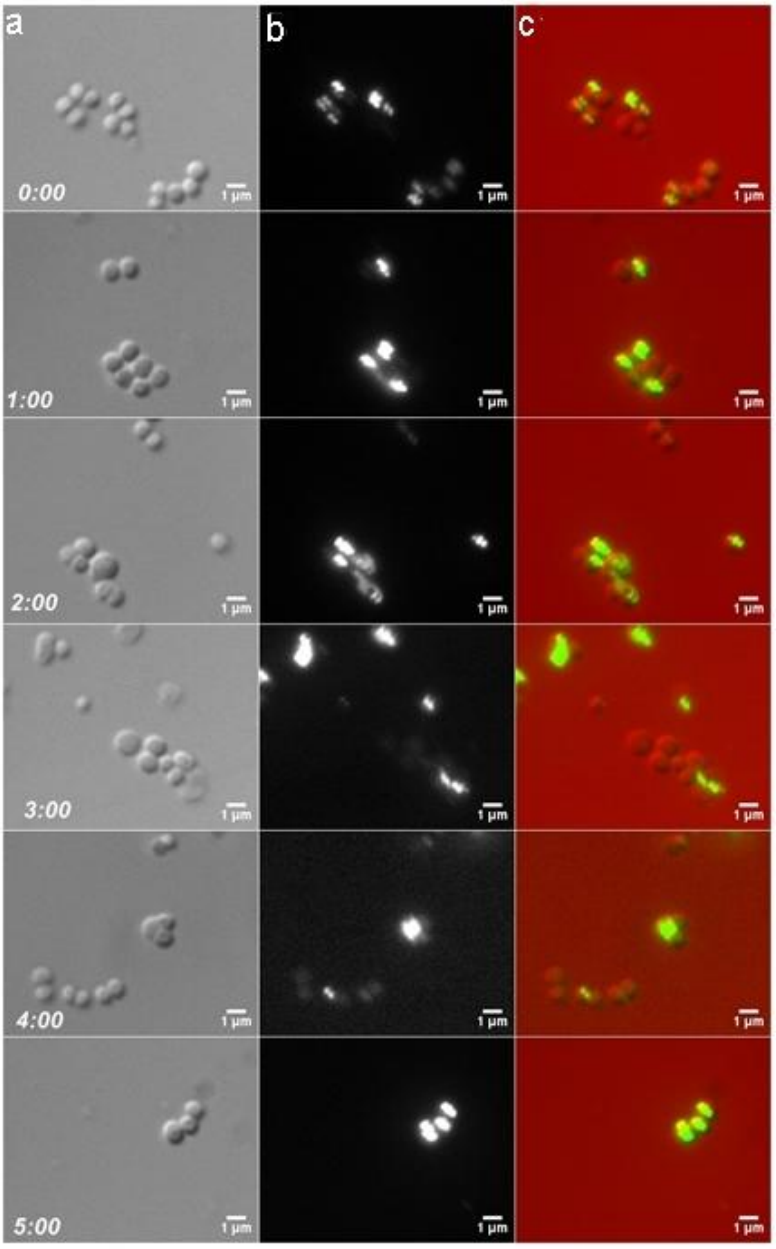

Figure 22: Effect of Hydroxyurea (25 mM) treatment on cells. a- Time series (0:00 – 5:00) of DIC images of *S.aureus* cells treated with Hydroxyurea (25 mM) with 0:00 hrs- untreated. b- Florescent images of DAPI stained nucleoids. c- Overlay of florescent image in green with DIC images in red. Scale bar =1 µm**.**

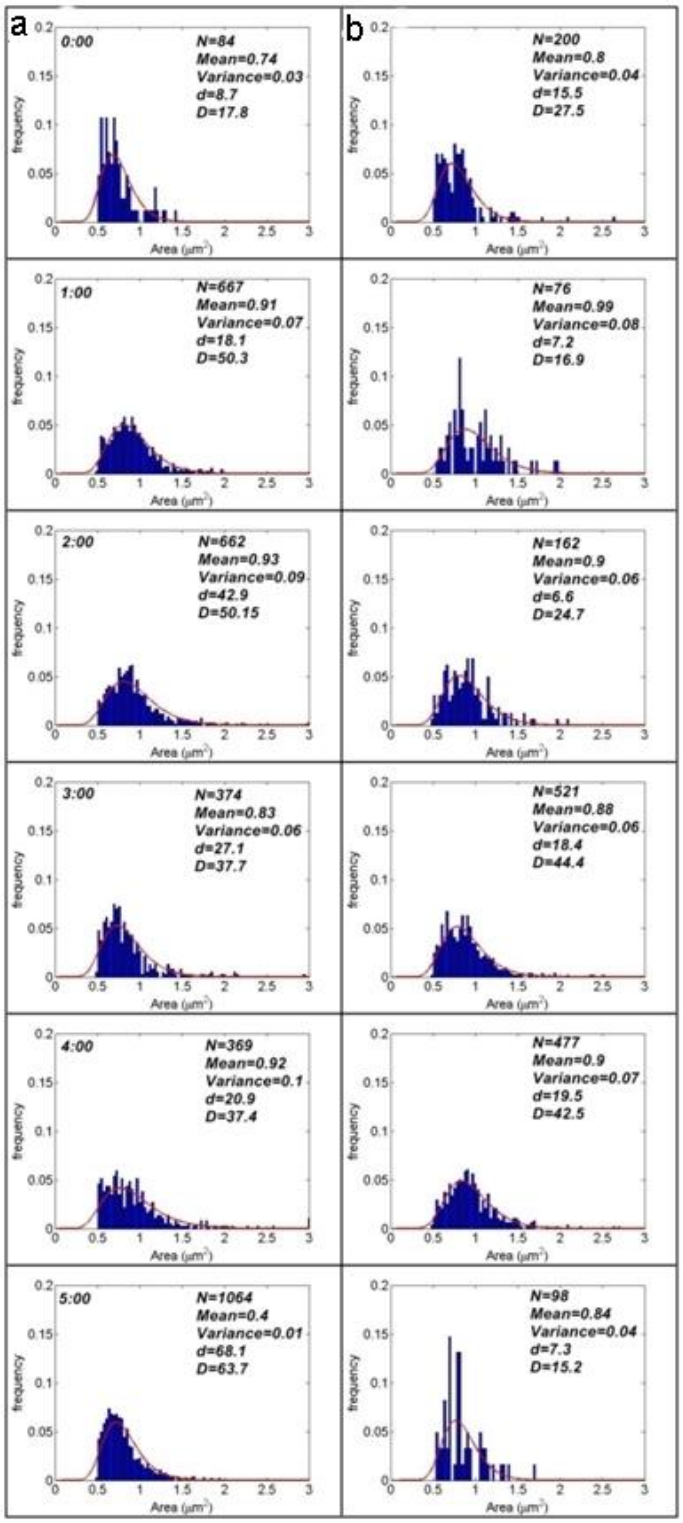

Figure 23: Frequency distribution plots of areas of cells treated with Hydroxyurea (HU). Area histograms of treated with 10 mM (Panel a) and 25 mM (Panel b) Hydroxyurea. Areas on X axis in μm^2, frequency (sum normalized) on Y axis. N-number of samples analyzed,

Mean- Mean of the samples, Variance- Variance of the samples, D- test statistic (Eq. 5), d- deviation from the fit (Eq. 6).

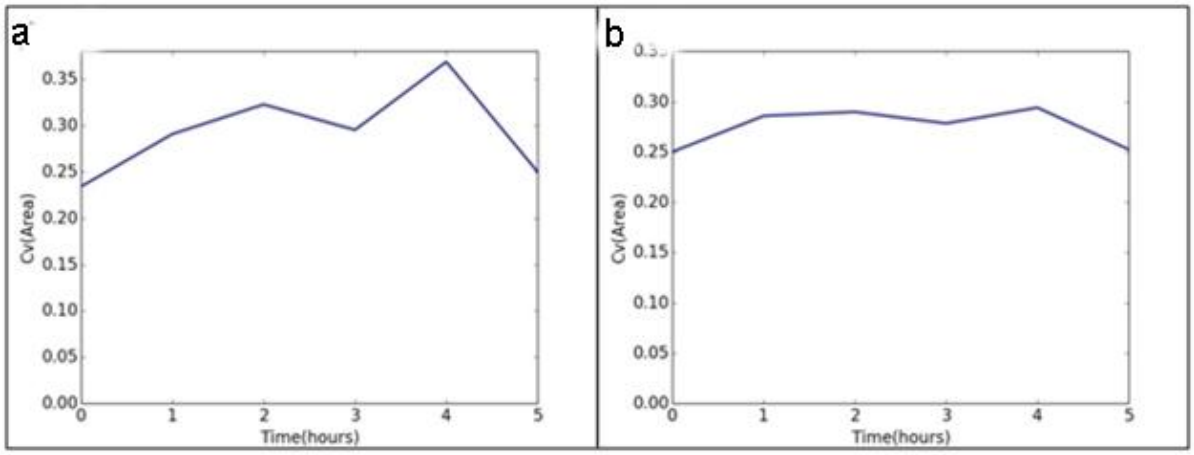

Figure 24: Coefficient of variation (CV) plots of Hydroxyurea treated cells. Hydroxyurea treated samples, a-10 mM and b-25 mM. Time (hours) on X-axis and Coefficient of Variation (CV) of area on Y-axis.

Recovery after Hydroxyurea Treatment

Cells treated with Hydroxyurea (after 3 hours of treatment) were recovered (washed and re-suspended in fresh NB). Nucleoids of cells were segregated in the cells seen after two hours of treatment (Figure 24b and Figure 25b); however significant difference in mean cell length was not seen and surprisingly means cell area is found to be increasing in the samples collected after 2 hours of recovery from both treatments. (Figure 26)

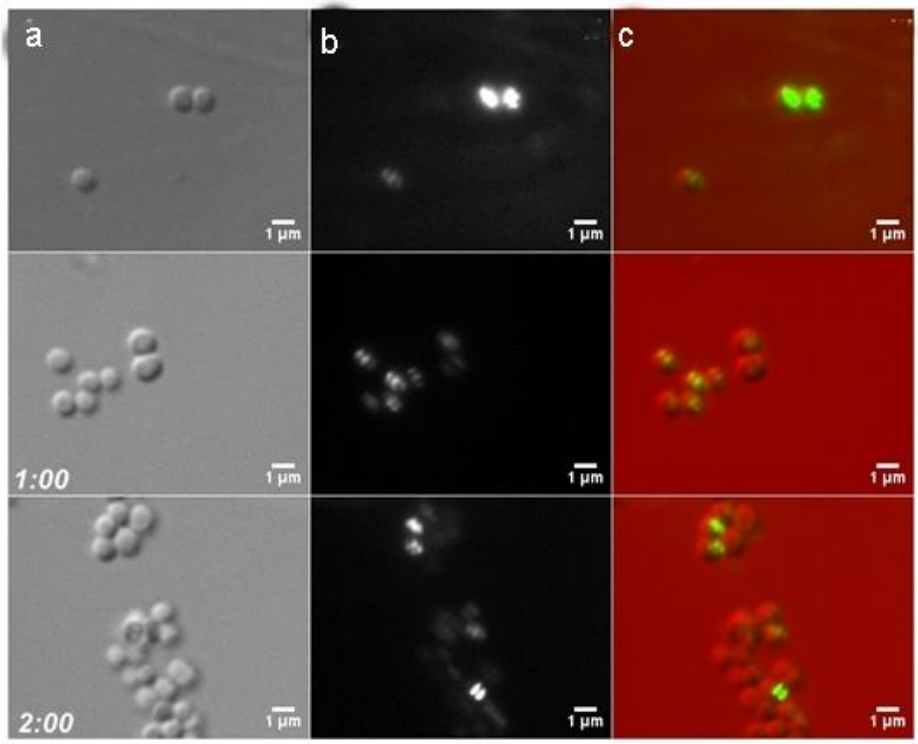

Figure 25: Recovery of cells after Hydroxyurea treatment (10 mM).a- Time series (from top to bottom) of DIC images of *S.aureus* cells recovered after Hydroxyurea (10 mM) treatment with image in upper panel- treated. b- Florescent images of DAPI stained nucleoids. c- Overlay of florescent image in green with DIC images in red. Scale bar =1 µm.

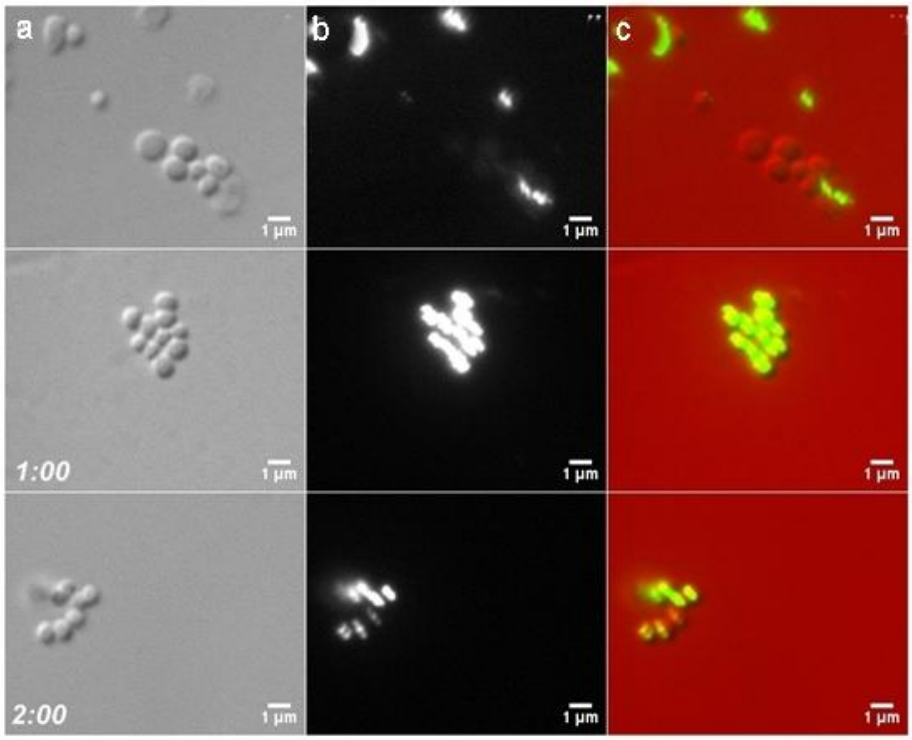

Figure 26: Recovery of cells after Hydroxyurea treatment (25 mM).a- Time series (from top to bottom) of DIC images of *S.aureus* cells recovered after Hydroxyurea (25 mM) treatment with image in upper panel- treated. b- Florescent images of DAPI stained nucleoids. c- Overlay of florescent image in green with DIC images in red. Scale bar =1 µm.

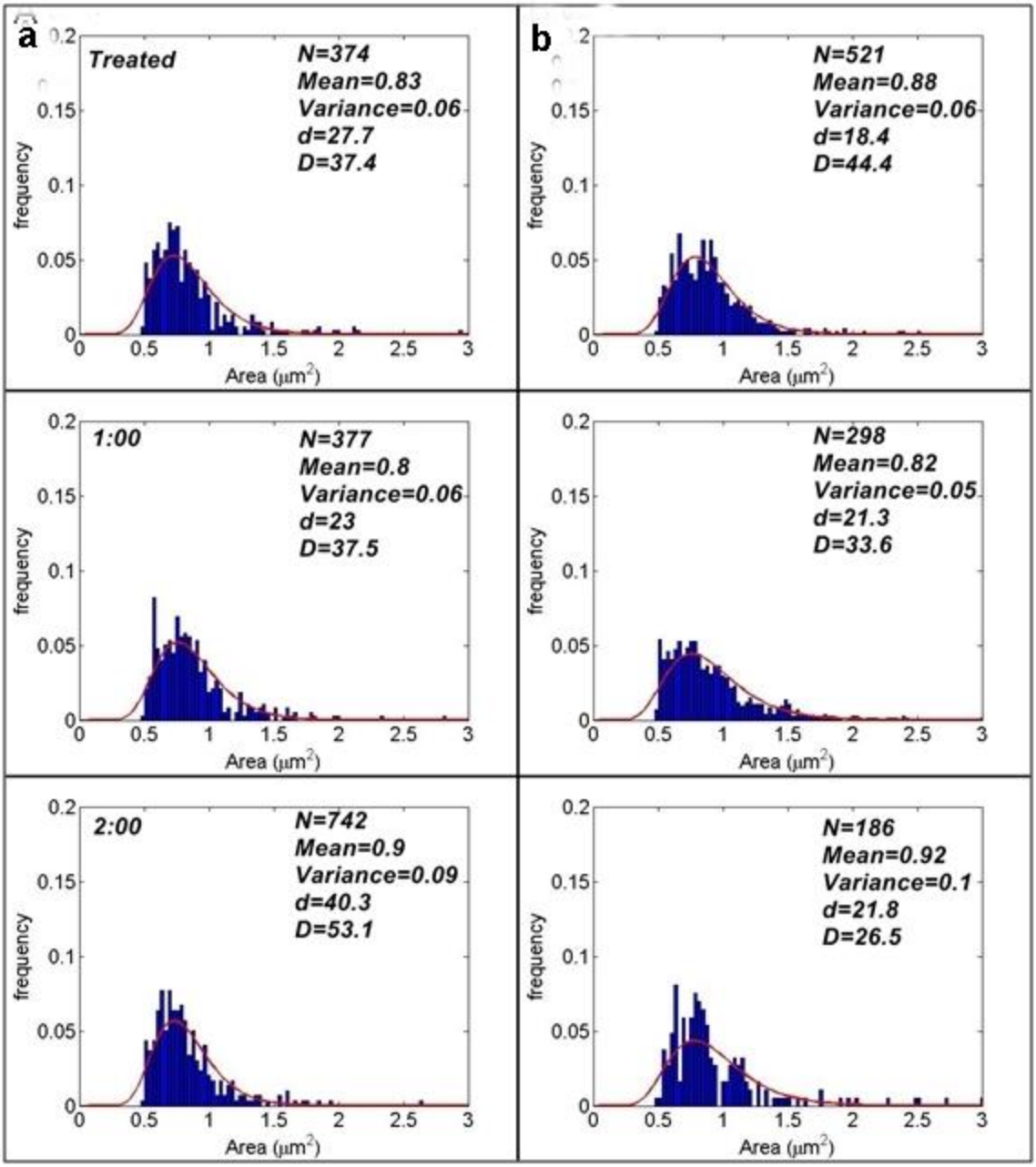

Figure 27: Frequency distribution plots of areas of cells recovered after Hydroxyurea treatment. Area histograms of recovered cells after treatment with 10 mM (Panel a) and 25 mM (Panel b) Hydroxyurea with treated cells distributions in topmost panel. Areas on X axis in μm^2, frequency (sum normalized) on Y axis. N-number of samples analyzed, Mean- Mean of the samples, Variance- Variance of the samples, D- test statistic (Eq. 5), d- deviation from the fit (Eq. 6).

Discussion

Our algorithm detects cell sizes in *S.aureus* in DIC and is used to distinguish cells with abnormally enlarged area in the population. Slope of the straight line fitted for manually measured (considered as standard) area against areas estimated by using an algorithm is 1.01 with 1% error (Figure 7). The validation of our algorithm using beads showed, 7.4% error in the size measurement (Eq. 8), which leads to an offset of 0.074 µm from the actual diameter of the object. This indicates that the cell size assessment by algorithm is accurate with submicron level error. Occasionally code detects few out of focus cells as seen in figure 27a outlined in figure 27b and in binarized image (Figure 27c), we have set a size filter to eliminate cells having area <0.5 μm^2, since ideal area of *S.aureus* is known to be 0.75 μm^2 (Touhami et al., 2004). However, this algorithm can be used only for 2-D image analysis.

Modulation of growth rate by diluting the growth media (1:10 and 1:30 dilution of NB with PBS) did not show much difference in the phenotypic noise in population. In contrast with our earlier studies with the batch cultures of *E. coli*, we did not observe significant difference in the variability in the cell size of the same population across different growth phases.

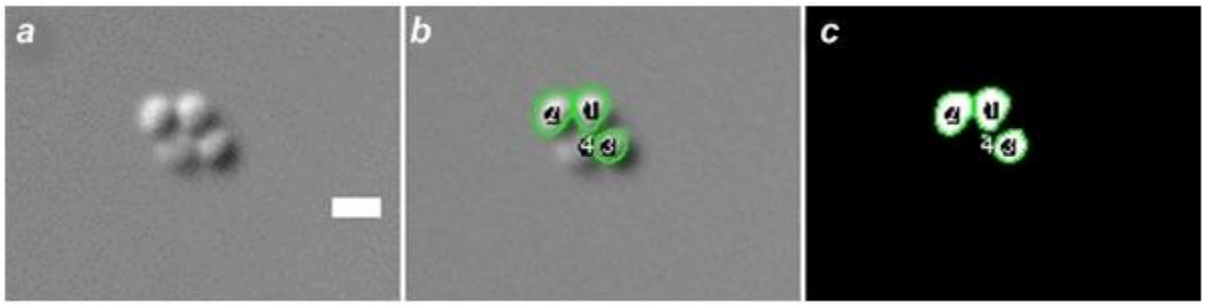

Figure 28: Detection of out of focus cells by algorithm. DIC images of cells- a, labeled – b showing out of focus cell (no.4). Detected images of cells by algorithm, along with the labels-c**.**

Upon Cephalexin treatment, the average of the cell size distribution shifts towards the higher value, as expected. Surprisingly, we did not observe inflation in the noise values. Similar results were obtained when the culture was treated with Hydroxyurea. In fact, we observed recovery in the average value of the distribution after 5 hrs. We also could observe normal nucleoid segregation after 5 hours of drug treatment. We think of the possibility of normal growth of survivors or resistant cells in a medium after 5:00 hours of drug treatment may lead to the decrease in cell size variability. Based on our findings, we predict that *S. aureus* has stronger mechanism for cell size homeostasis.

Taken together an algorithm developed in our lab measures cell area accurately. However, it requires further improvements in order to be able to analyze cells in three dimensions. Also, we aim to develop a code to detect nucleoids in bacterial cells as DNA dynamics plays pivotal role in cell size maintenance.

References

Amir, A. (2014). Cell size regulation in bacteria. Phys. Rev. Lett. *112*, 1–5.

Athale, C. a, and Chaudhari, H. (2011). Population length variability and nucleoid numbers in Escherichia coli. Bioinformatics *27*, 2944–2948.

Bernard, R., Marquis, K.A., and Rudner, D.Z. (2010). Nucleoid occlusion prevents cell division during replication fork arrest in Bacillus subtilis. Mol. Microbiol. *78*, 866–882.

Bernhardt, T.G., and De Boer, P.A.J. (2005). SlmA, a nucleoid-associated, FtsZ binding protein required for blocking septal ring assembly over chromosomes in E. coli. Mol. Cell *18*, 555–564.

Bi, E., and Lutkenhaus, J. (1993). Cell division inhibitors SulA and MinCD prevent formation of the FtsZ ring. J. Bacteriol. *175*, 1118–1125.

Chien, A., Hill, N.S., and Levin, P.A. (2012). Cell size control in bacteria. Curr. Biol. *22*, R340–R349.

Elowitz, M.B., Levine, A.J., Siggia, E.D., and Swain, P.S. (2002). Stochastic gene expression in a single cell. Science *297*, 1183–1186.

Freed, N.E., Silander, O.K., Stecher, B., Böhm, A., Hardt, W.D., and Ackermann, M. (2008). A simple screen to identify promoters conferring high levels of phenotypic noise. PLoS Genet. *4*, 2–7.

Jones, L.J.F., Carballido-López, R., and Errington, J. (2001). Control of cell shape in bacteria: Helical, actin-like filaments in Bacillus subtilis. Cell *104*, 913–922.

Margolin, W. (2000). Themes and variations in prokaryotic cell division. FEMS Microbiol. Rev. *24*, 531–548.

Osella, M., Nugent, E., and Cosentino Lagomarsino, M. (2014). Concerted control of Escherichia coli cell division. Proc. Natl. Acad. Sci. U. S. A. *111*, 3431–3435.

Pinho, M.G., and Errington, J. (2003). Dispersed mode of Staphylococcus aureus cell wall synthesis in the absence of the division machinery. Mol. Microbiol. *50*, 871–881.

Rasband, W.S. (2012). ImageJ.

Roerdink, J., and Meijster, a (2000). The Watershed Transform: Definitions, Algorithms and Parallelization Strategies. Fundam. Informaticae *41*, 187–228.

Schaechter, M., MaalOe, O., and Kjeldgaard, N.O. (1958). Dependency on Medium and Temperature of Cell Size and Chemical Composition during Balanced Growth of Salmonella typhimurium. J. Gen. Microbiol. *19*, 592–606.

Shehata, T.E., and Marr, A.G. (1975). Effect of temperature on the size of Escherichia coli cells. J. Bacteriol. *124*, 857–862.

Taheri-Araghi, S., Bradde, S., Sauls, J.T., Hill, N.S., Levin, P.A., Paulsson, J., Vergassola, M., and Jun, S. (2014). Cell-Size Control and Homeostasis in Bacteria. Curr. Biol. *25*, 385–391.

Todar, K. Online Textbook of Bacteriology. http://textbookofbacteriology.net/staph.html

Touhami, A., Jericho, M., and Beveridge, T. (2004). Atomic force microscopy of cell growth and division in Staphylococcus aureus. J. Bacteriol. *186*, 3286–3295.

Trueba, F.J., Spronsen, E. a Van, Traas, J., and Woldringh, C.L. (1982). Effects of Temperature on the Size and Shape of Escherichia coli Cells. Arch. Microbiol. *131*, 235–240.

Turner, R.D., Ratcliffe, E.C., Wheeler, R., Golestanian, R., Hobbs, J.K., and Foster, S.J. (2010). Peptidoglycan architecture can specify division planes in Staphylococcus aureus. Nat. Commun. *1*, 26.

Tzagoloff, H., and Novick, R. (1977). Geometry of cell division in Staphylococcus aureus. J. Bacteriol. *129*, 343–350.

Veiga, H., Jorge, A.M., and Pinho, M.G. (2011). Absence of nucleoid occlusion effector Noc impairs formation of orthogonal FtsZ rings during Staphylococcus aureus cell division. Mol. Microbiol. *80*, 1366–1380.

Watson, S.P., Clements, M.O., and Foster, S.J. (1998). Characterization of the starvation-survival response of Staphylococcus aureus. J. Bacteriol. *180*, 1750–1758.

Wilcox, R. (1998). Kolmogorov–Smirnov Test. Encycl. Biostat. 83–90.

Wu, L.J., and Errington, J. (2004). Coordination of cell division and chromosome segregation by a nucleoid occlusion protein in Bacillus subtilis. Cell *117*, 915–925.

Appendix

Cell size detection Algorithm devised in Image

```
//This script will read files from a folder and run the staph detection code

// Chaitanya &Priyatham

dir1 = getDirectory("Choose Source Directory ");
```

```
dir2 =  getDirectory("Choose Source Directory ");//dir1+"data\";  //output directory where analyzed data is saved

list = getFileList(dir1); //full list of file names in the directory- assuming only image data is present there.

//setBatchMode(true);

for (i=0; i<99; i++){    //list.length; i++) {

showProgress(i+1, list.length);

print(dir1+list[ i ] );

open( dir1+list[ i ] );

t=getTitle;

print(t);

detectBac();

resFile=dir2+list[i]+".txt";

print(resFile);

selectWindow("Results");

saveAs("Measurements",resFile);

            //rename(t +'_detect');

close();

}

//Priyatham 30-Jan-2014using OTSU

functiondetectBac() {

close();

run("8-bit");

run("Smooth");

run("Median...", "radius=2");

run("Maximum...", "radius=2");
```

```
run("Subtract Background...", "rolling=25");

run("OtsuThresholding ");

selectWindow("Threshold");

run("Watershed");

//run("Outline");

run("Analyze Particles...", "size=0-Infinity circularity=0.00-1.00 show=Nothing display exclude clear include  add");

}
```

Lognormal fit code to frequency histograms scripted in Matlab.

```
close all; clear all;
clf; close all;
% read in the data
a=importdata ('.txt');%%input text file
z= find (a (:,1)>=0.5); %filter
a3= a (z)
N = length (a3);% no. of samples
N
% plot the experimental data based on a histogram
x=linspace (0,3,100); % x-vals
% experimental data freq. distr
% if (a>0.5)
 [p,q]=hist (a3,x);
% else
%     continue
% end
p1=p./max(p); % max normed
p2=p./sum(p); % sum normed
% figure (1),hold on, subplot (1,2,1), bar (q,p1,'b'),title ('max normed')
figure (1),bar (q,p2,'b')%,title ('sum normed')
```

```
%== FIT
% create an x-axis range of lengths for the fit based on the min-max of data
b=linspace (min (a3),max (a3),30);
% fit a lognormal distribution
pd=fitdist (a3,'lognormal');
% generate the pdf of the fit
y=lognpdf (q,pd.mu,pd.sigma);% plot the pdf as a function of the x-vals
y2= y./sum(y);% sum normed (area under curve = 1)
```

```
% extract the logn parameters (mu, var)
[M,V]=lognstat (pd.mu,pd.sigma)
```

```
% figure (1), hold on, subplot (1,2,1),plot (q,y,'-r'),legend ('Expt','Fit'),
% xlabel ('length'),ylabel ('freq');

figure (1), hold on, plot (q,y2,'-r','linewidth',2)%,legend ('Expt','Fit'),
xlabel ('Area (\mum^2)','fontsize',16),ylabel ('frequency','fontsize',16),...
set (gca,'XTick',([0:0.5:5]),'fontsize',16,'YTick',([0:0.05:0.3]),'fontsize',16);
% text (max (q)/1.2,3*max (y2)/2,sprintf ('N=%2 .2f','M=%2 .2f','V=%2 .2f'N,M,V));
xlim ([0,3])
ylim ([0,0.2])

% cumulative sum used to calculate chi-square statistic
p3=cumsum (p2);
% figure (2), plot (q,p3,'-ob');% O: observed

% cumulative sum of the fit
y3=cumsum (y2);
% hold on, plot (q,y3,'-xr');% E: expected
% legend ('Observed','Expected')
% text (4,1.2,sprintf ('No. of observed classes: % i',length (q)));
% here n=no. of classes
% hence: df = n - 1

% chi-square statistic
SSD = sum ((((p3-y3).*N).^2)./(N.*y3));
SSD;
df = length (q)-1; % degrees of freedom

% xlim ([0,10]);
% ylim ([0,1.5]);
%[h,p,st]=chi2gof (a,'cdf',pd);
% myCdf = [q',N.*y3'];
% myObs = [q',p2'];% pdf supplied
%[h,p,ksstat] = kstest (N.*p3',myCdf, 0.05,'unequal');

F1=N*p3;
F2=N*y3;
d=F1-F2;
max (d)
```

$$D = \mathrm{sqrt}((-\log(0.001/2))/2 * N)$$